Portable IR dye laser optofluidic microresonator as a temperature and chemical sensor

F. Lahoz,[1,2,*] I. R. Martín,[1,3] J. Gil-Rostra,[4] M. Oliva-Ramirez,[4] F. Yubero,[4] and A. R. Gonzalez-Elipe[4]

[1]*Departamento de Física, Universidad de La Laguna, San Cristóbal de La Laguna, Santa Cruz de Tenerife, 38200, Spain*

[2]*Instituto de Estudios Avanzados en Atómica, Molecular y Fotónica (IUDEA), Universidad de La Laguna, San Cristóbal de La Laguna, Santa Cruz de Tenerife, 38200, Spain*

[3]*MALTA Consolider Team, Instituto de Materiales y Nanotecnología (IMN), Universidad de La Laguna, San Cristóbal de La Laguna, Santa Cruz de Tenerife, 38200, Spain*

[4]*Nanotechnology on Surfaces Laboratory. Instituto de Ciencia de Materiales de Sevilla (CSIC-Univ. Sevilla). Avda. Américo Vespucio 49. 41092 Sevilla, Spain*

[*]*flahoz@ull.es*

Abstract: A compact and portable optofluidic microresonator has been fabricated and characterized. It is based on a Fabry-Perot microcavity consisting essentially of two tailored dichroic Bragg mirrors prepared by reactive magnetron sputtering deposition. The microresonator has been filled with an ethanol solution of Nile-Blue dye. Infrared laser emission has been measured with a pump threshold as low as 0.12 MW/cm^2 and an external energy conversion efficiency of 41%. The application of the device as a temperature and a chemical sensor is demonstrated. Small temperature variations as well as small amount of water concentrations in the liquid laser medium are detected as a shift of the resonant laser modes.

OCIS codes: (140.2050) Dye lasers; (140.3410) Laser resonators; (140.3948) Microcavity devices; (280.4788) Optical sensing and sensors.

References and links

1. F. P. Schäfer, W. Schmidt, and J. Volze, "Organic dye solution laser," Appl. Phys. Lett. **9**(8), 306–309 (1966).
2. M. J. Weber, *Handbook of Laser Science and Technology Supplement 2: Optical Materials (Laser & Optical Science & Technology)* (CRC, 1995).
3. C. Sanchez, B. Lebeau, F. Chaput, and J.-P. Boilot, "Optical properties of functional hybrid organic-inorganic nanocomposites," Adv. Mater. **15**(23), 1969–1994 (2003).
4. S. Chénais and S. Forget, "Recent advances in solid-state organic lasers," Polym. Int. **61**(3), 390–406 (2012).
5. H. Schmidt and A. R. Hawkins, "The photonic integration of non-solid media using optofluidics," Nat. Photonics **5**(10), 598–604 (2011).
6. W. Wang, C. Zhou, T. Zhang, J. Chen, S. Liu, and X. Fan, "Optofluidic laser array based on stable high-Q Fabry-Pérot microcavities," Lab Chip **15**(19), 3862–3869 (2015).
7. M. C. Gather and S. H. Yun, "Single-cell biological lasers," Nat. Photonics **5**(7), 406–410 (2011).
8. T. Wienhold, S. Kraemmer, S. F. Wondimu, T. Siegle, U. Bog, U. Weinzierl, S. Schmidt, H. Becker, H. Kalt, T. Mappes, S. Koeber, and C. Koos, "All-polymer photonic sensing platform based on whispering-gallery mode microgoblet lasers," Lab Chip **15**(18), 3800–3806 (2015).
9. X. Fan and S. H. Yun, "The potential of optofluidic biolasers," Nat. Methods **11**(2), 141–147 (2014).
10. Y. Chen, L. Lei, K. Zhang, J. Shi, L. Wang, H. Li, X. M. Zhang, Y. Wang, and H. L. W. Chan, "Optofluidic microcavities: Dye-lasers and biosensors," Biomicrofluidics **4**(4), 043002 (2010).
11. X. Fan and I. M. White, "Optofluidic microsystems for chemical and biological analysis," Nat. Photonics **5**(10), 591–597 (2011).
12. B. Helbo, A. Kristensen, and A. Menon, "A micro-cavity fluidic dye laser," J. Micromech. Microeng. **13**(2), 307–311 (2003).
13. Z. Li, Z. Zhang, A. Scherer, and D. Psaltis, "Mechanically tunable optofluidic distributed feedback dye laser," Opt. Express **14**(22), 10494–10499 (2006).
14. H. Zhu, I. M. White, J. D. Suter, P. S. Dale, and X. Fan, "Analysis of biomolecule detection with optofluidic ring resonator sensors," Opt. Express **15**(15), 9139–9146 (2007).
15. S. I. Shopova, H. Y. Zhou, X. D. Fan, and P. Zhang, "Optofluidic ring resonator based dye laser," Appl. Phys. Lett. **90**(22), 221101 (2007).

#263671 Received 20 Apr 2016; revised 17 May 2016; accepted 22 May 2016; published 16 Jun 2016

16. Y. Gong, M. Zhang, C. Gong, Y. Wu, Y. Rao, and X. Fan, "Sensitive optofluidic flow rate sensor based on laser heating and microring resonator," Microfluid. Nanofluidics **19**(6), 1497–1505 (2015).
17. M. R. Foreman, J. D. Swaim, and F. Vollmer, "Whispering gallery mode sensors," Adv. Opt. Photonics **7**(2), 168–240 (2015).
18. Q. Chen, M. Ritt, S. Sivaramakrishnan, Y. Sun, and X. Fan, "Optofluidic lasers with a single molecular layer of gain," Lab Chip **14**(24), 4590–4595 (2014).
19. Y. Sun, S. I. Shopova, C. S. Wu, S. Arnold, and X. Fan, "Bioinspired optofluidic FRET lasers via DNA scaffolds," Proc. Natl. Acad. Sci. U.S.A. **107**(37), 16039–16042 (2010).
20. F. Lahoz, C. J. Oton, D. López, J. Marrero-Alonso, A. Boto, and M. Díaz, "Whispering gallery mode laser based on antitumor drug-dye complex gain medium," Opt. Lett. **37**(22), 4756–4758 (2012).
21. F. J. Duarte, *High-Power Dye Lasers* (Springer Verlag, 1991), Ch. 4.
22. S. Balslev and A. Kristensen, "Microfluidic single-mode laser using high-order Bragg grating and antiguiding segments," Opt. Express **13**(1), 344–351 (2005).
23. Q. Kou, I. Yesilyurt, and Y. Chen, "Collinear dual-color laser emission from a microfluidic dye laser," Appl. Phys. Lett. **88**(9), 091101 (2006).
24. Q. Kou, I. Yesilyurt, G. Escalier, J. C. Galas, L. Coureau, and Y. Chen, "Microfluidic dye laser integration in a lab-on-a-chip device," Proc. SPIE **5641**, 112–115 (2004).
25. F. Lahoz, C. J. Oton, D. López, J. Marrero-Alonso, A. Boto, and M. Díaz, "High efficiency amplified spontaneous emission from a fluorescent anticancer drug–dye complex," Org. Electron. **14**(5), 1225–1230 (2013).
26. B.-B. Li, Q.-Y. Wang, Y.-F. Xiao, X.-F. Jiang, Y. Li, L. Xiao, and Q. Gong, "On chip, high-sensitivity thermal sensor based on high-Q polydimethylsiloxane-coated microresonator," Appl. Phys. Lett. **96**(25), 251109 (2010).
27. C.-H. Dong, L. He, Y.-F. Xiao, V. R. Gaddam, S. K. Ozdemir, Z.-F. Han, G.-C. Guo, and L. Yang, "Fabrication of high-Q polydimethylsiloxane optical microspheres for thermal sensing," Appl. Phys. Lett. **94**(23), 231119 (2009).
28. L. L. Martín, C. Pérez-Rodríguez, P. Haro-González, and I. R. Martín, "Whispering gallery modes in a glass microsphere as a function of temperature," Opt. Express **19**(25), 25792–25798 (2011).
29. R. J. Riobóo, M. Philipp, M. A. Ramos, and J. K. Krüger, "Concentration and temperature dependence of the refractive index of ethanol-water mixtures: influence of intermolecular interactions," Eur Phys J E Soft Matter **30**(1), 19–26 (2009).
30. F. Sedlmeir, R. Zeltner, G. Leuchs, and H. G. L. Schwefel, "High-Q MgF_2 whispering gallery mode resonators for refractometric sensing in aqueous environment," Opt. Express **22**(25), 30934–30942 (2014).
31. V. D. Ta, R. Chen, D. M. Nguyen, and H. D. Sun, "Application of selfassembled hemispherical microlasers as gas sensors," Appl. Phys. Lett. **102**(3), 031107 (2013).
32. H. Li and X. Fan, "Characterization of sensing capability of optofluidic ring resonator biosensors," Appl. Phys. Lett. **97**(1), 011105 (2010).

1. Introduction

Organic dye lasers have been largely investigated since their first demonstration in the sixties [1]. Dye molecules are π-conjugated, have a broad emission band, which enables tunability of the laser emission, and show a high quantum yield of the fluorescence. They have been frequently used in solutions as liquid lasers [2], or incorporated in host polymer matrices, as solid-state lasers [3, 4].

More recently, optofluidics has attracted great interest as an emerging field in photonics, which combines fluidic gain media with solid resonant structures to achieve integrated optical devices, including high quality lasers [5–7]. One of the most promissing application of these devices is as optical sensors, showing high sensitivities and integration capabilities [8–11]. In most cases, laser dye solutions are injected in the optofluidic device through external mechanic pumping. This is required to provide a continuous flow to avoid photobleaching, which is the main drawback of dye liquid lasers for practical applications. The first demonstration of a microcavity dye laser reported a pulsed pump laser threshold of above 30 MW/cm^2 [12]. It was based on a simple Fabry-Perot (FP) microresonator with two metallic thin layers to accomplish optical feedback. A significant reduction of the pump threshold (0.1 MW/cm^2) was achieved in a distributed feedback (DFB) optofluidic laser. However, the implementation of the device required micro-engineering to fabricate a Bragg grating embedded in the liquid core [13]. Further decrease of the pump threshold has been demonstrated using whispering gallery mode (WGM) resonators [14, 15]. Moreover, WGM resonators have been widely investigated for their promising sensor applications in fields such as chemistry, physics or biology [11, 16–20].

#263671 Received 20 Apr 2016; revised 17 May 2016; accepted 22 May 2016; published 16 Jun 2016

In this paper, we report on the fabrication and characterization of a simple and compact optofluidic dye laser based on a FP microresonator. Nile-Blue (NB) dye molecules have been chosen as the gain medium and near infrared (NIR) laser emission has been demonstrated. Pump threshold as low as 0.1 MW/cm^2 has been measured using this simple architecture. Moreover, external conversion efficiency as high as 41% has been observed, which is comparable to the conversion efficiency of commercially available dye laser devices, such as rhodamines, under optical pulsed excitation [21]. In addition to this, no photobleaching has been observed even without flow of the dye solution through the microcavity. The device is compact and portable. It shows good optical results and the fabrication process is easy. All these features are appealing for applications, such as temperature or chemical sensors. Indeed, variations around human body temperature are detected through shift of the resonant laser modes. Futhermore, small contents of water in the optofluidic laser medium were analyzed by detection of the shift of the laser wavelengths, as it is shown in the last part of the paper.

2. Experimental

2.1 Device Fabrication

The layout of the optofluidic system used as laser resonator cavity is shown in Fig. 1(a). It consists of a sealed volume delimited by two parallel fused silica plates covered with dichroic Bragg mirrors separated by approximately 150 microns. The dye solution in this cavity can be replaced by circulation through tubing fittings located in one of the plates. The sealing material was PDMS. The two Bragg mirrors covering the inner sides of the plates consisted of multilayer systems rendering different optical responses.

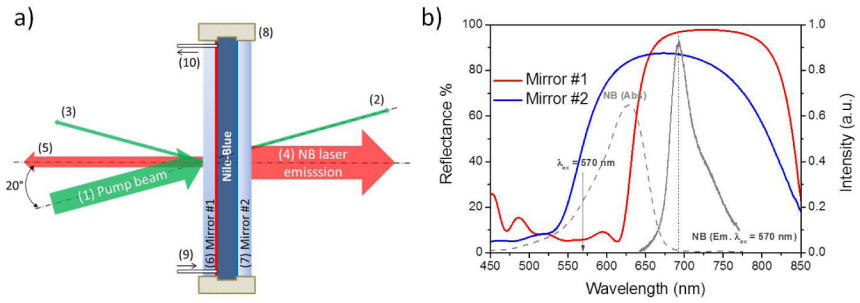

Fig. 1. (a) Scheme of the optofluidic laser resonator device (not at scale):): **(1)** Laser pump beam (570 nm), **(2)** transmitted pump beam (4%), **(3)** reflected pump beam (14%), **(4)** Nile-Blue forwards laser emission (74%), **(5)** Nile-Blue backward s laser emission (26%), **(6)** mirror #1, **(7)** mirror #2, **(8)** 150 microns spacer, **(9)** and **(10)** in/out tubing fittings. (b) Reflectance spectra of mirror #1 (red) and mirror #2 (blue) (front and back inner surfaces) and normalized absorption (dashed grey) and PL emission spectra (solid grey) of NB dye in ethanol (1 mM). The excitation wavelength at 570 nm is indicated with an arrow.

According to Fig. 1(b), mirror #1 was designed to provide a high reflectance, ~96%, at the maximum of the emission spectra of the NB dye, about 700nm, and a low reflectance, ~5%, in a wide band region encompassing the absorption band of the NB dye between 550 and 620 nm. Mirror#2 was broader and had a reflectance of about 85% in a region that encompasses the maximum of the absorption and emission spectra of the NB dye. Laser excitation was made by light of 570 nm through the plate coated with mirror #1 as indicated in the Fig. 1(b). This optical performance for the Bragg mirrors was achieved by stacking a series of high refractive index Nb_2O_5, n@550nm = 2.29, and low refractive index SiO_2, n@550nm = 1.46, layers with the following thickness distribution:

Mirror #1: (40 nm SiO_2/150 nm Nb_2O_5/40 nm SiO_2)x 7.

Mirror #2: (40 nm SiO_2/90 nm Nb_2O_5/40 nm SiO_2)x 4.

#263671 Received 20 Apr 2016; revised 17 May 2016; accepted 22 May 2016; published 16 Jun 2016

Where the factors 7, mirror #1, and 4, mirror #2, stand for the number of repetitions of the basic stack under parentheses. The definition of the number of layers, their thickness and the stack architecture was determined by simulation with a WVASE software code.

The Nb_2O_5 and SiO_2 thin film layers of the Bragg reflectors were sequentially deposited by reactive magnetron sputtering using, respectively, niobium and silicon targets (75 mm diameter) and a source operated with a pulsed DC power supply (AE Pinnacle Plus +) and a power of 215 W for Nb_2O_5 films and 185 W for SiO_2 films (frequency 120 KHz, reverse time 2.5 μs). The samples were prepared at 150°C and the magnetron target-substrate distance was approximately 10 cm. The process gas consisted of a mixture of Ar (40 sccm) and O_2 (4 sccm) at a pressure of $5.0 \cdot 10^{-3}$ mbar.

2.2 Dye composition and laser experiments

A solution of about 2 ml of NB dye in ethanol at a concentration of 1 mM was prepared. The dye solution was poured into a cuvette for some preliminary photoluminescence (PL) characterization or it was injected into the FP device for the laser experiments.

A pulsed optical parametric oscillator, OPO, (10 Hz, 8 ns pulse width) tuned at about 570 nm, close to the maximum absorption of the NB dye solution, was used as the excitation source. The pump beam was focused onto the sample using a 100 mm focal length spherical lens to form an excitation pump spot of about 300 μm diameter, which represented a pump area of about 7.07×10^{-4} cm^2.

The PL of the dye was collected with a high numerical aperture optical fiber coupled to a CCD spectrometer. The best spectral resolution of the spectrometer was 0.1 nm.

For the laser experiments the pump beam was at an angle of about 20° from the surface normal direction to avoid alignment with the NB laser emission. In the laser efficiency experiments, a calibrated silicon detector (Ophir PD300R-3W) was used to measure both the pump and the output laser energy per pulse.

In the temperature sensor experiments the FP laser device was submerged in a temperature controlled water bath. The water container had glass walls, transparent both to the excitation beam and to the NIR laser output, which could be easily detected out of the water bath. The temperature range was from 25°C to 45°C. Higher temperature was not achieved to avoid damage in the FP device sealing polymer.

Solutions of NB dissolved in mixtures of ethanol and water were prepared to demonstrate the capability of the NB FP laser device as a chemical sensor. The water content ranged from 0 up to 20 mol% (equivalent to 0.072 vol%). The FP device was rinsed three times with pure ethanol when the NB laser solution was changed.

3. Results and discussion

3.1 Laser emission

The PL of a solution of 1 mM NB in ethanol poured in a quartz cuvette under excitation at around 570 nm is given in Fig. 2(a) (i). It shows the characteristic broad emission band of NB centred at about 695 nm, with a full width at half maximun (FWHM) of around 70 nm. This PL band is due to spontaneous emission. Its shape does not change when the pump power is increased and it does not depend on the detection direction. However, when the same solution is injected in the FP device the behaviour of the emission is completely different. If the PL emission is detected at normal direction under low pump power, the emission spectrum is formed by the superposition of the typical broad emission band of NB and a set of nearly equally spaced narrow lines, which are due to constructive interference of the optical modes of the FP cavity at the spectral range of the emission band, see Fig. 2(a) (ii). Moreover, when the pump intensity is increased above a certain threshold the emission spectrum abruptly changes showing only the narrow peaks associated to the FP cavity modes, see Fig. 2(a) (iii). The width of the resonant lines is about 0.1 nm, and it is limited by the spectral resolution of

#263671 Received 20 Apr 2016; revised 17 May 2016; accepted 22 May 2016; published 16 Jun 2016

the experimental setup. On the contrary, if the PL emission of the FP device is detected at a collection angle away of the normal direction the narrow cavity mode lines are not detected at any pump power below or above pump threshold.

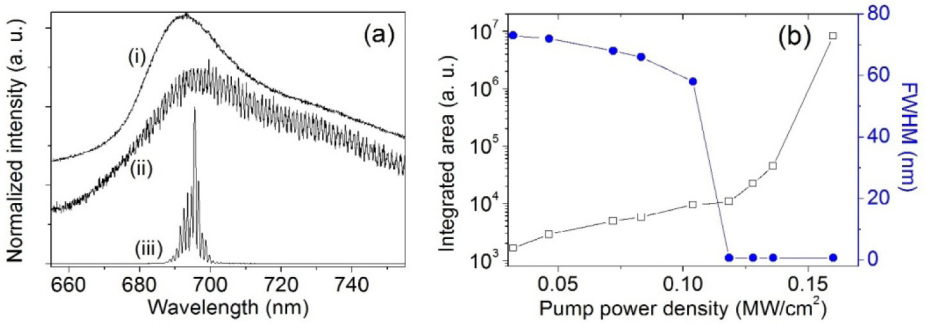

Fig. 2. (a) Normalized emission spectra of the NB dye solution (i) in a cuvette; in the laser device under (ii) 0.08 MW/cm^2 and (iii) 0.16 MW/cm^2 pump power. Spectra have been vertically shifted for clarity. (b) Emission intensity (black squares) and FWHM (blue circles) as a function of the pump power.

In addition to this, the intensity of the emission at normal direction dramatically increases at the pump threshold. The evolution of the integrated spectral emission intensity measured at normal direction and the reduction of the FWHM as the pump power density increases is given in Fig. 2(b). Both the narrowing of the emission band and the increase of the emission intensity at the pump threshold demonstrate that it is due to laser emission with a pump threshold as low as 0.12 MW/cm^2, which corresponds to a pump energy density of 9.6 x 10^3 nJ/mm^2. It is noticeable that this is a relatively low pump threshold for a FP microcavity, and it is comparable to laser threshold values reported for DFB lasers, which required more complicated structures such as a Bragg grating embedded in a single mode microfluidic channel waveguide [13]. Moreover, the slope of laser emission vs pump intensity indicates that the external energy conversion efficiency of the FP laser cavity is as high as 41%, see Fig. 3(a). If the output laser intensity is plotted against the absorbed pump power, which is about 82% of the pump, an internal laser efficiency of 50% is obtained. These values are outstandingly high for a FP microcavity, especially the external efficiency parameter, and are comparable to optimized and commercially available liquid dye lasers [21]. A laser threshold of about 0.4 MW/cm^2 has been reported, for instance, in optofluidic dye lasers based on distributed feedback high order Bragg grating fabricated by lithographic techniques on a polymer layer [22]. Moreover, the laser output efficiency was only around 1%. A similar laser threshold of about 0.4 MW/cm^2 has been reported for a FP microcavity made with gold mirrors [23, 24]. Nevertheless, the output laser efficiency is not reported and a continuous flow rate above 2μL/min is required to avoid bleaching of the dye laser emission. Recently, very low laser thresholds of only 0.002 and 0.022 MW/cm^2 have been reported for a high-Q plano-concave and plano-plano FP microcavities, respectively [6]. The plano-concave arquitecture provides a more stable microcavity, which significantly reduces the laser threshold. However, even the plano-plano FP microcavity shows a very low pump threshold. In order to achive this low pump power parameter high reflectiviy coatings (>99.9%) have been used. The authors report a laser threshold of 0.17 MW/cm2 for a similar plano-plano FP microcavity but with lower reflectivity coatings (> 99.5%) [6]. This seems to suggest that we could improve the laser threshold of our FP device by increasing the reflectivity of the Bragg coatings.

A study of the performance of the FP cavity as a function of the concentration of the dye gain medium is out of the purpose of this research and has not been made. Moreover, the concentration and the dye used by different authors were not the same as those used in this

#263671 Received 20 Apr 2016; revised 17 May 2016; accepted 22 May 2016; published 16 Jun 2016

paper [6, 13, 22–24]. Consequently, direct comparisons of the performance parameters are not straightforward. However, the previous discussion is enough to show that both the laser threshold and especially the laser emission efficiency of the FP device are very interesting for such a device.

Concerning the measured high value of the laser efficiency, we believe that it is related to the fact that photobleaching of the dye emission was not observed in the FP device even without flow of the solution, as it will be shown later. The relatively high thickness of the cavity (~170 μm) means a dye solution volume high enough to continuously provide dye molecules that replace those, which could be damaged after intense pump pulses. This prevents photoinduced optical losses in the microcavity and allows the high laser efficiency observed. In a previous work, we have observed a similar behaviour in optically induced liquid channel waveguide. High efficiency (30%) amplified spontaneous emission was observed in a dye solution without photobleaching [25].

The laser device is multimode and the wavelengths at which the resonances occur correspond to the FP cavity modes. They depend on the refractive index of the medium n, and the thickness of the cavity, d, as:

$$m\lambda_m = 2nd. \tag{1}$$

Where m represents the mode number. The refractive index of the dye solution is considered to be practically equal to that of the solvent, ethanol, which is 1.3587. The thickness of the cavity (about 170 μm) has been estimated from comparison of absorbance measurements using a calibrated solution. This value is higher than that of the 150 μm spacers used in the fabrication of the cavity. We think that this can be due to partial penetration of the PDMS holder polymer into the cavity borders. According to this result and Eq. (1), the mode number of each laser line could be assigned and it is given in Fig. 3(b).

The free spectral range (FSR) is defined as the wavelength difference between two successive cavity modes. It is given by:

$$FSR = \frac{\lambda^2}{2nd}. \tag{2}$$

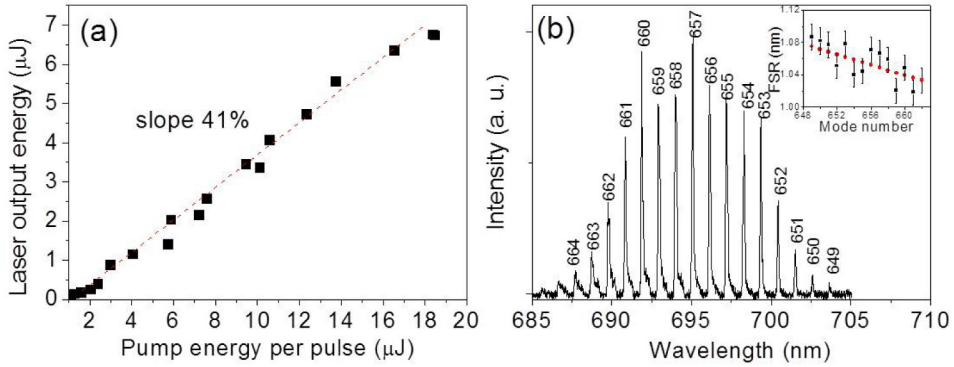

Fig. 3. (a) Laser emission as a function of the incident pump energy. Dashed red line is a linear fit. (b) IR laser modes. Mode numbers are indicated. Inset gives the experimental (black squares) and simulated (red circles) FSR vs mode number.

The best fit of Eq. (2) to the experimentally observed FSR data is obtained for a d value of 168 μm, see inset of Fig. 3(b), in good agreement with the value obtained previously.

An estimation of a lower limit value of the quality factor (Q-factor) of the cavity can be made as $\nu_0/\Delta\nu$, where ν_0 is the resonant frequency and $\Delta\nu$ is the FWHM. Taking into account the laser modes shown in Fig. 3(b) a Q-factor of around 7.6 x 10^3 is obtained. As it has

#263671 Received 20 Apr 2016; revised 17 May 2016; accepted 22 May 2016; published 16 Jun 2016

already been mentioned, this provides just a lower limit because the spectral linewidths of the resonant modes are limited by the resolution of the experimental setup.

Another characteristic of the laser emission is its directionality. It has already been mentioned that the narrow lines associated to the FP cavity modes could not be detected under low pump power excitation when the detection was out of the normal direction. Moreover, above the pump threshold, the NB laser emission showed a high directionality. The output laser beam was normal to the reflecting surfaces, as it can be observed in the picture of Fig. 4(a). The divergence of the laser emission was measured and it was around ± 11 mrad.

An important drawback of dye lasers is photobleaching. In oder to avoid it, continuous flow of dye solution is frequently required. However, in spite of the small volume of the laser cavity (around 68 μL), no detectable photobleaching of the laser signal was observed at least after 18000 pump pulses (which is equivalent to 30 min of OPO excitation) at a significant pump density of 21 mJ/cm^2 (equivalent to 2.6 MW/cm^2), see Fig. 4(b). As it has already been discussed the volume of the gain medium acts as a reservoir that renews the dye molecules in pump region preventing photobleaching.

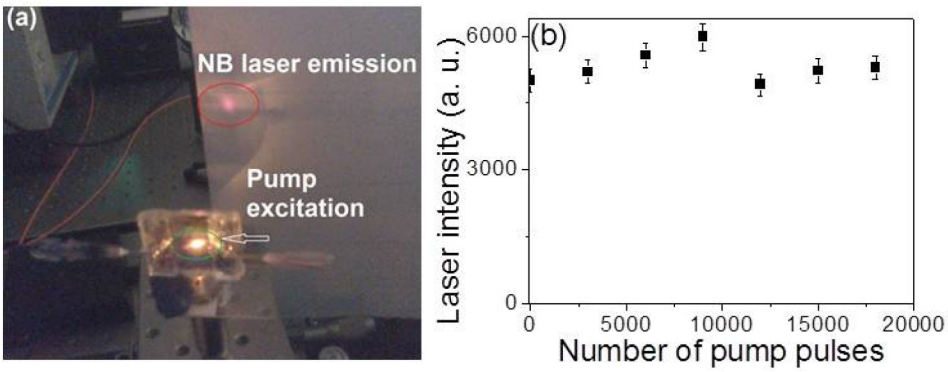

Fig. 4. (a) Photograph of the dye laser portable device under laser operation. The output IR laser beam is indicated in the picture. (b) Intensity of the IR laser emission as a function of the number of excitation pump pulses.

In summary, all these data show that a portable, compact, and efficient FP laser can be easily fabricated and implemented using a commercial dye solution and two dichroic mirror surfaces prepared by magnetron sputtering deposition of a multilayer stack. Moreover, a much broader laser spectral range from the visible to the NIR could be obtained with a set of FP cavities designed with reflecting coatings adapted for different laser dyes.

3.2 Temperature sensor

These small, compact and efficient microlasers can be used as sensors of different parameters, which have an influence on any of the characteristic features of the laser output emission. In particular, temperature has an influence on the refractive index of the laser medium and the laser emission wavelength depends directly on n (see Eq. (1)). Consequently, a shift of the laser peaks should be expected as the temperature changes.

It is known that n decreases for ethanol as temperature increases according to [14]:

$$n = 1.36890 - 0.00041T. \tag{3}$$

where T is the temperature in Celsius degrees.

Therefore, a blue shift of the laser lines is likely to occur when T increases. If this spectral shift can be measured and calibrated in a range of temperature, the FP cavity laser can be used as a temperature sensor.

#263671 Received 20 Apr 2016; revised 17 May 2016; accepted 22 May 2016; published 16 Jun 2016

As a proof of concept, the FP cavity was tested as follows. It was submerged into a temperature controlled water bath. The needles were sealed to avoid any NB solution leakage. The cavity could be optically excited through the water bath and the laser emission was carefully recorded out of the water container. A blue shift of the laser lines was observed as temperature was increased. The spectral positions of the laser lines, which correspond to the mode numbers 653 and 661, are given in Fig. 5 together with the theoretical prediction according to Eqs. (1) and (3), red and black squares, respectively. A relative disagreement between experimental data and theory can be observed, which could indicate that the resonant mode also depends on other factors, such as cavity thermal expansion. In any case, these results demonstrate that due to the narrow width of the laser modes, a tiny increment of temperature can be detected through a blue shift of the laser lines, which could be interesting for example, for non-invasive biological applications. The results show a thermal sensitivity of about 0.15 nm/°C. A similar value of 0.151 nm/°C was reported for a toroidal resonator coated with a layer of polydimethylsiloxane (PDMS) [26]. A higher sensitivity of 0.245 nm/ °C was found using PDMS microspheres [27]. In both references the sensors are based on high-Q WGM resonators, which are fabricated with PDMS because it is a material that shows a high thermo-optic coefficient, dn/dT [17]. The sensitivity reported, for instance, in Nd3 + doped microspheres is 10 pm/°C, an order or magnitude below our device [28]. Concerning the sensor resolution of the FP device, we estimate that the temperature variation limit, which can be detected with our experimental spectral resolution is about 1.5 °C. This corresponds to a laser line shift of 0.2 nm, which we establish conservatively as the limit of detection of the shift of the cavity modes. The sensor resolution value is relatively low as compared to the high-Q PDMS WGM resonators, for which a resolution of the order of 10^{-4} °C is reported [26, 27]. However, in those cases, the WGM shift was monitored by a wavelength-swept laser-based optical spectrum analyser with a resolution of 0.2 pm. On the other hand, as it has already been mentioned, the measured spectral width of the cavity laser modes of our FP device, 0.1 nm, is limited by the spectrometer. Therefore, if higher resolution could be achieved, the temperature resolution would be correspondingly improved.

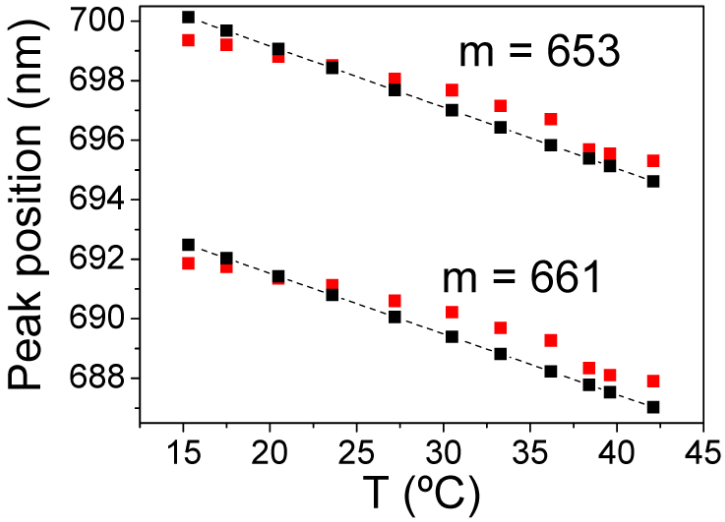

Fig. 5. Evolution of the laser peak positions as a function of temperature for two different laser modes (red squares). Black squares and dashed lines give the simulated peak positions (see the text).

#263671 Received 20 Apr 2016; revised 17 May 2016; accepted 22 May 2016; published 16 Jun 2016

3.3 Chemical sensor

The value of n, at a given temperature, is basically determined by the solvent composition. Therefore, the wavelength position of a cavity mode changes if the NB dye is dissolved in different solvents. In particular, mixing of water and ethanol is especially interesting because some anomalies in the refractive index of the mixture have been explained in terms of segregation and clustering of water an ethanol molecules. Moreover, in spite of the fact that the refractive index of water is lower than that of ethanol, an increase of n has been reported in solutions of mixtures of ethanol with a low content of water [29].

Four different solutions were prepared to demonstrate the capability of the microcavity laser to be used as a sensor of water in a mixture of x mol% H_2O-(100-x) mol% Ethanol, where x was 0 (pure ethanol), 2.5, 5, 10 and 20.

According to [29] n increases as the amount of water in the mixture is higher. As a consequence, the expected value of resonant wavelength of a given cavity mode should be red shifted when the water concentration is augmented. Figure 6 shows, as an example, the wavelength of mode m = 653 at T = 21°C, for the four mixtures. A continuous shift to higher wavelength values is detected if the water content is increased. Moreover, the wavelength positions predicted from Eq. (1) using the n values reported in [29] are included. The experimental data follow the tendency of the theoretical prediction, although some quantitative disagreement can be observed. This can be due to differences in the purity of the solvents used in our experiment and in [29], which has an impact in the refractive index. Indeed, ethanol solvent used in our experiments was stored in ambient conditions and therefore, contamination with water molecules present in the surrounding atmosphere cannot be disgarded. Consequently, the real water concentration could be about 4 mol% higher than estimated. This means a better matching of our experimental results with those predicted from the n values reported in [29]. These measurements are based on the dependence of the laser line position on the refractive index. According to Eq. (1) a refractive index variation limit of 0.0004 can be estimated, which corresponds to a laser line shift of 0.2 nm. As already said, if the spectral resolution of the experimental setup would be improved, the detection limit would be even lower.

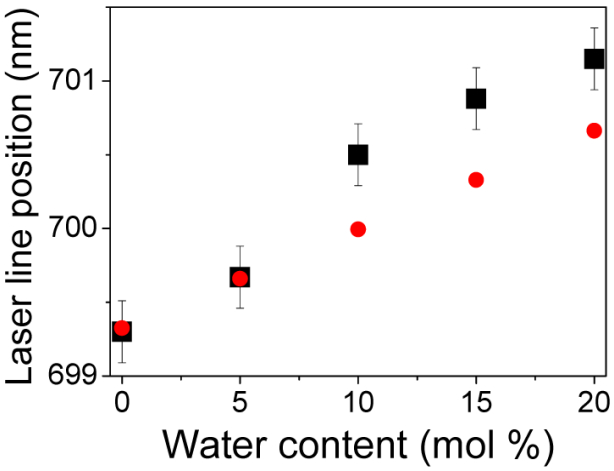

Fig. 6. Dependence of the experimental (black squares) and theoretical (red circles) laser peak position on the water content of the solution.

Both chemical and temperature sensors are based on the wavelength shift of the microcavity resonant modes when the refractive index of the liquid medium is changed. As an example of the sensitivity of the optofluidic FP cavity, it can be expressed as wavelength change of the modes over refractive index unit (RIU) change. In the case of the m = 653

#263671 Received 20 Apr 2016; revised 17 May 2016; accepted 22 May 2016; published 16 Jun 2016

resonant mode, a sensitivity of 514 nm/RIU can be obtained from Eq. (1). A value of 3.26 nm/RIU has been reported for a high-Q crystalline MgF_2 WGM resonator [30]. A higher figure of 130 nm/RIU has been found in selfassembled Rhodamine B doped PMMA hemispherical microlasers [31]. A similar value of 570 nm/RIU has been detected in a capillary-based optofluidic ring resonator [32]. In addition to all these results, the fact of using liquid lasers in FP cavities offers some advantages over other temperature and refractive index measurement methods. First, they are easily fabricated and integrated in optofluidic systems, which is becoming a promising biosensing technology [9–11]. In addition to this, this approach can be used for fluorescent biological probes such as cells genetically modified to express fluorescent proteins [7], or purified enzyme/protein solutions labelled with a fluorophore. These biological samples can be circulated through the FP cavity and their laser emission used as a temperature/chemical sensor or even to analyze other induced processes.

4. Conclusions

A compact NIR dye microresonator laser has been fabricated and characterised. It is formed by a FP microcavity filled with a NB solution, which can be easily replaced with a syringe. Under optical excitation at the maximum of the NB absorption band, the laser emission shows a pump threshold as low as 0.12 MW/cm^2. The external energy conversion efficiency of the laser is 41% and the internal efficiency reaches 50%. These features are among the best reported for dye lasers [21].

This small device is portable and does not require delicate alignment for laser operation. Even if the gain medium has a low volume of just 68 μL, no photobleaching has been detected after 18000 excitation pulses. Consequently, external pipes and gain solution pumping system are not necessary for laser operation, which increases the portability of the device compared to other continuous flow optofluidic devices. To obtain more portable devices, the external excitation laser could be replaced by a visible semiconductor laser to pump the dye molecules. Therefore, the fact that the laser device is stable and portable makes it appealing for biological applications, for which NIR laser sources are required for deep penetration in human tissues. Moreover, different wavelength ranges can be achieved using adequate dye lasers and adjusting the design of the FP reflecting layers. In this way, laser emission through the visible and NIR range can be accomplish just by easily changing the FP cavity in the experimental setup.

As an example of the applications of the microcavity laser, the use of the FP cavity as a temperature sensor has been demonstrated. Small temperature variations around human body temperature can be detected and measured by a shift of the resonant laser lines. In addition to this, the FP laser was implemented as a chemical sensor for the detection of small volumes of solvents such as water. The spectral shift of the resonant wavelength of the laser modes was used to detect water content.

The easy of the fabrication of these efficient, portable and stable laser devices makes them appealing as laser sources. Besides, they offer the possibility to cover visible and NIR spectral range with a set of FP cavities and dye lasers, which broadens their applications, such as temperature and chemical sensors.

Acknowledgments

This research was supported by MINECO (MAT2013-40852-R), (MAT2013-46649-C4-4-P), the Consolider-Ingenio 2010 Program MALTA (CSD2007-0045) and FUNCOAT + (MAT2015-69035-REDC), by the EU-FEDER, and by the Junta de Andalucía (projects P12-FQM-2265 and P10-FQM-6900).

#263671 Received 20 Apr 2016; revised 17 May 2016; accepted 22 May 2016; published 16 Jun 2016